


Original article

Controllable electromechanical stability of a torsional micromirror actuator with piezoelectric composite structure under capillary force

Mingjia Liu¹, Yonglin Chen¹, Wen Cheng², Siyu Chen¹, Tao Yu¹, Weidong Yang¹ *

¹School of Aerospace Engineering and Applied Mechanics, Tongji University, Shanghai 200092, P. R. China

²Department of Materials Science and Engineering, National University of Singapore, Singapore 117575, Singapore

Keywords:

Micromirror actuator
capillary force
pull-in instability
torsional piezoelectric composite

Cited as:

Liu, M., Chen, Y., Cheng, W., Chen, S., Yu, T., Yang, W. Controllable electromechanical stability of a torsional micromirror actuator with piezoelectric composite structure under capillary force. *Capillarity*, 2022, 5(3): 51-64.
<https://doi.org/10.46690/capi.2022.03.02>

Abstract:

Various types of micro/nano functional devices are being widely designed as optical switches, micro scanners, micromirrors and other core optical devices. The continuing miniaturization of the functional devices makes the size dependence of electromechanical property significant in micro/nano scale due to the sharp increase of surface interactions such as capillary force from liquid bridge, van der Waals and Casimir forces from quantum fluctuations. The surface interactions can cause the pull-in instability, adhesion between parts, and even failure of device. This work provides an active control method to avoid the pull-in instability of an electrostatically driven circular micromirror by applying voltage on a torsional piezoelectric composite structure. The influences of the three types are compared of dispersion forces on the electromechanical stability of the micromirror actuator. A comprehensive electromechanical model of a torsional piezoelectric beam was established to numerically investigate the electromechanical coupling of the micromirror. The results show that the influence of capillary force on the stability of the micromirror is as significant as van der Waals force and Casimir force. By introducing piezoelectric nanoplates into the laminated torsional structure, the micromirror stability can be controlled based on the piezoelectric effect of the torsional piezoelectric composite structure. This work can contribute to the structural optimization design and manufacture of micromirror systems.

1. Introduction

With the rapid development of micro/nano processing technology, micro-optical electromechanical system, known as optical micro electromechanical system (MEMS), has been widely used in optical switches (Takabayashi et al., 2021; Xu and Younis, 2022), micro scanners (Wang et al., 2020; Fang et al., 2022), micromirrors (Tang et al., 2022) and other core optical devices. Specifically, a torsional micromirror system usually consists of a pair of elastic beams providing torsional deformation, a micromirror driven by an electrical/optical signal and a substrate to support them (Khatami and Rezazadeh, 2009). The micromirror will tilt under the electrostatic force

generated by external voltage. Then, the beams attached on the micromirror will be twisted and generate a reaction torque to balance the micromirror at a certain tilting angle, which can be regarded as a deformation indicator and gives feedback to the input electrical signal of the operating device systems. However, once the external voltage exceeds a critical value, the pull-in instability phenomenon of the micromirror system will occur, that is, the micromirror will jump and be suddenly adsorbed to the substrate (Yang et al., 2021).

The pull-in instability is one of the most important mechanical problems in MEMS, which may be caused by the structural design and manufacturing methods of MEMS (Afrang et al., 2019; Kumar et al., 2020; Yang et al., 2021). Therefore,

this phenomenon has attracted much attention recent years. Some researchers proposed mathematical models to describe the pull-in instability, which provides important criteria for designing stable MEMS (Daeichin et al., 2020; Tian et al., 2022). Researchers also presented methods to prevent the phenomenon. For example, Tian et al. designed fractal models in porous structures to transform the pull-in instability into a stable state (Tian et al., 2021; Tian and He, 2021).

Traditional electromechanical manufacturing process of sensors and actuators in the rapid development of the Internet has been difficult to match most scenarios. Volume, efficiency, high quantity production costs, and production efficiency are all disadvantages that cannot be overcome, while small size and high performance are the core advantages of MEMS devices. However, MEMS size decreases continually and corresponding specific surface area increases, which lead to obvious surface effect. The significant increase in specific surface area and the relative increase in the number of atoms on the surface of the particles make these surface atoms highly reactive and highly unstable, resulting in the particles exhibiting different properties, which is the surface effect. The influence of surface interatomic forces, such as van der Waals (vdW) force, Casimir force confirmed by Lamoreaux et al. (1997) and capillary force, will become more and more significant. These forces act on micromirror systems in different principles. VdW force and Casimir force are generated by the fluctuation effect of the vacuum electromagnetic field. Casimir force can be regarded as a hysteresis vdW force, with a more extended force range than vdW force. While, the capillary force is generated by the residual liquid in the manufacturing process or in the air when a liquid bridge is built in the MEMS. Even so, all of them can lead to pull-in instability of micromirror systems in advance. Therefore, studying the effect of surface forces on the electromechanical stability of micromirror systems can help in the fabrication and control of the systems and other MEMS.

Among these surface forces, Casimir forces has been widely considered in the pull-in instability characteristics of electrostatic-driven MEMS. Recently, Chen et al. (2019) reported a novel energy dissipation mechanism of nanomechanical resonators induced by the Casimir effect, in which the energy loss due to the Casimir effect plays an important role in the dissipation of the nanobeam resonator. Masoumi et al. (2021) also found that electrostatic driving force with edge field effect and Casimir force affects the nonlinear static introduction instability of smart nano-switches. Other studies showed that ignoring Casimir force leads to significant overestimation of pull-in voltage of micro-actuators (Bhojawala and Vakharia, 2017, 2020; Yang et al., 2017c).

In addition to vdW force and Casimir force, capillary force persists even at the lowest relative humidity (van Zwol et al., 2008). The modified LW equation for various microchannels and porous media is useful for understanding capillary imbibition across different types of porous systems (Cai et al., 2021). A comprehensive review modeling infiltration processes in capillaries was systematically presented, through which a roadmap for infiltration of capillaries with arbitrary and complex geometries can be predicted (Cai et al., 2022). Although capillary force has been studied in steady-state or

dynamic systems such as porous structures (Liang et al., 2020; Li et al., 2021; Cai et al., 2022), it is rarely studied in MEMS. Tang et al. (2022) found that capillary force often appears between the micromirror and the substrate of MEMS actuators. In many cases, such as wet etching process, the effect of capillary force on actuator stability becomes more significant and is needed to be investigated comprehensively (Yang et al., 2017a; Sun et al., 2021).

To avoid the pull-in instability and make MEMS controllable, piezoelectric materials have attracted more and more interest and used in various electromechanical applications (Chang et al., 2012; Yang et al., 2022), such as piezoelectric ceramics, polyvinylidene fluoride (Ico et al., 2016; Jariwala et al., 2021) and piezoelectric composites (Curry et al., 2020; Le et al., 2022). The characteristics of piezoelectric materials involves the positive piezoelectric effects in which the piezoelectric voltage is converted into mechanical energy, and the inverse piezoelectric effect in which the mechanical energy is converted into piezoelectric voltage. Based on these effects, Yang et al. (2016, 2017b) proposed a manipulative approach to control the pull-in state and enhance the structural reliability of electrostatic nano-devices with a piezoelectric layer. Additionally, a MEMS micromirror driven by integrated piezoelectric (PZT) film was also demonstrated, and a design law of improving the performance of piezoelectric-driven MEMS micromirror can be obtained through theoretical analysis (Opreni et al., 2021).

In this study, the aim is to form a feedback protection mechanism to protect MEMS devices. In section 2, a theoretical model of an electrically actuated micromirror system is firstly constructed, and the electrostatic torque as well as the surface torques acting on the micromirror were derived. Then, a piezoelectric composite structure torsion beam with piezoelectric sheets is designed, for generating torques to counteract or balance out the excessive torques. In section 4, the finite element model of the micromirror system is established and numerical solution is computed via COMSOL Multiphysics platform. Finally, the mechanical stability and pull-in instability of the piezoelectric micromirror system were analyzed considering the surface forces, especially the capillary force. By using the piezoelectric beam, not only the tilting angle of the micromirror can be sensed, but the stability of it can also be controlled.

2. Theoretical model of electrically actuated micromirror

A single degree of freedom micromirror mechanical model is established as shown in Fig. 1(a). A circular rotatable main plate (i.e., a micromirror) is firmly attached with elastic torsional beams on both sides. They are supported by two rigid anchors fixed on a substrate. Fixed electrodes are laid on the substrate under the main plate. In the model, the bending deformation of the rotatable plate and torsional beam is ignored. As shown in Fig. 1(b), the only degree of freedom of the micromirror is the tilting angle θ . The radius of the main plate is R and the distance between the main plate and the fixed electrodes is d .

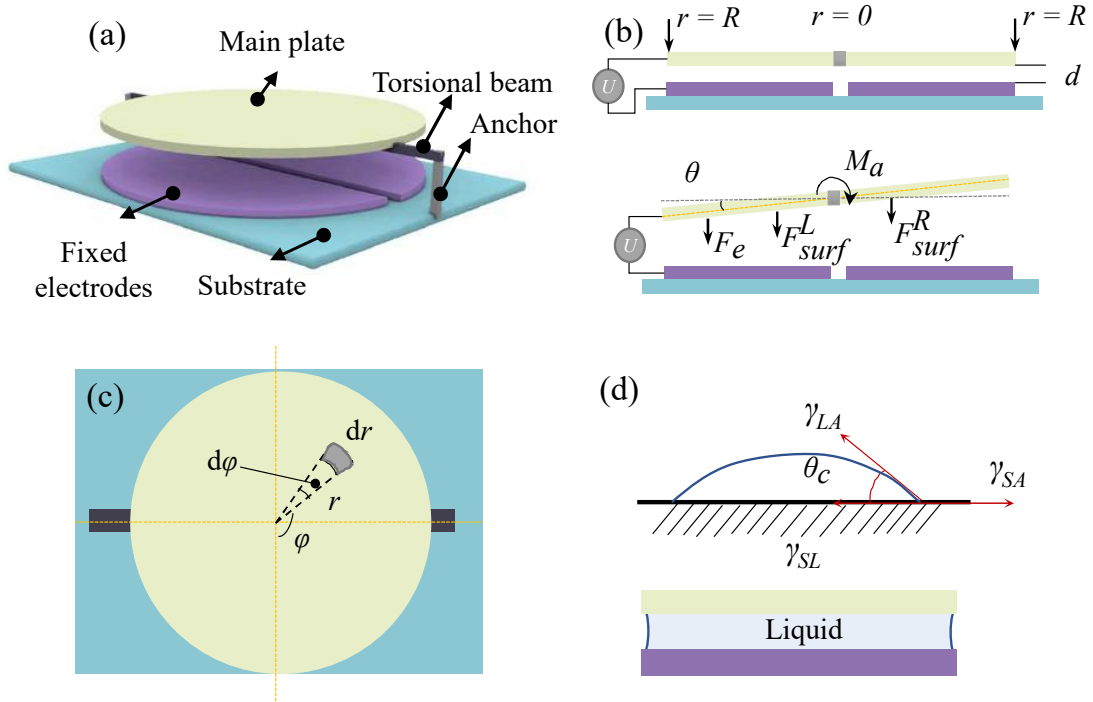


Fig. 1. Schematic diagram of micromirror system: (a) Composition of the micromirror system, (b) Side view and force analysis of micromirror system, (c) Top view of micromirror system, and (d) Schematic diagram of capillary force.

When the voltage is applied to one of the fixed electrodes, an electrostatic attraction F_e will be generated between the main plate and the fixed electrode and then drive the main plate to tilt as shown in Fig. 1(b). The infinitesimal element of the electrostatic force F_e (Fig. 1(c)) can be described as:

$$dF_e = \frac{\epsilon_0 V_e^2}{2(d - r \sin \theta \sin \varphi)^2} r dr d\varphi \quad (1)$$

Then, the infinitesimal element of the corresponding electrostatic torque M_e is:

$$\begin{aligned} dM_e &= r \cos \theta \sin \varphi dF_e \\ &= \frac{\epsilon_0 V_e^2}{2(d - r \sin \theta \sin \varphi)^2} r^2 \cos \theta \sin \varphi dr d\varphi \end{aligned} \quad (2)$$

where $\epsilon_0 = 8.854 \times 10^{-12} \text{ C}^2\text{N}^{-1}\text{m}^{-2}$ is the permittivity of vacuum, V_e is the applied electrostatic voltage, r and φ denote the radial and circumferential components of the circular main plate in the polar coordinate system, respectively (Fig. 1(c)). The electrostatic torque can be obtained by integrating Eq. (2), as expressed:

$$M_e = \frac{\epsilon_0 V_e^2 \cos \theta}{2 \sin^3 \theta} \left(\frac{2d^2 - R^2 \sin^2 \theta}{\sqrt{d^2 - R^2 \sin^2 \theta}} A - 4R \sin \theta - 2\pi d \right) \quad (3)$$

where $A = \pi + 2 \arctan \left(\frac{R \sin \theta}{\sqrt{d^2 - R^2 \sin^2 \theta}} \right)$. Since the micromirror tilting angle is small, $\sin \theta \approx \theta$ and $\cos \theta \approx 1$, Eq. (3) can be further simplified to:

$$M_e = \frac{\epsilon_0 V_e^2}{2\theta^3} \left(\frac{2d^2 - R^2 \theta^2}{\sqrt{d^2 - R^2 \theta^2}} B - 4R\theta - 2\pi d \right) \quad (4)$$

where $B = \pi + 2 \arctan \left(\frac{R\theta}{\sqrt{d^2 - R^2 \theta^2}} \right)$. However, when the

characteristic size of the micromirror system is reduced to an extent in micro and nano scales, the effect of the surface forces becomes significant, which may result in the system becoming unstable even if no external voltage is applied. According to the Fig. 1(b), the regime of electrostatic force covers one half of the main plate while the surface forces dominate the entire main plate.

If the main plate and the fixed electrodes remain parallel, then the torques of the surface forces on the fixed torsional nanobeam are zero, and they do not exert rotational torque on the rotatable main plate. Once the main plate is rotated by an angle θ , the surface torques are no longer zero. The beam is supposed to have torsional deformation, while the circular main plate only has rigid rotation under surface interactions.

The capillary torque provided by the capillary force is derived currently. As shown in Fig. 1(d), for a drop of liquid placed on a solid surface, γ_{LA} , γ_{SA} , and γ_{SL} represent the tension between liquid-air, solid-air, and solid-liquid interfaces, respectively. To maintain equilibrium, a contact angle θ_c is formed and Young's equation is satisfied:

$$\gamma_{SA} = \gamma_{SL} + \gamma_{LA} \cos \theta_c \quad (0 < \theta_c < \pi) \quad (5)$$

When there is a liquid bridge between the rotating main plate and the fixed electrodes, capillary force emerges between them, as shown in the Fig. 1(d). Since the main liquid invaded in MEMS is water, the liquid material considered in this paper for the capillary action is water (Zhang et al., 2016; Pal et al., 2021). The capillary action on the micro elements on the left dF_p^L and right dF_p^R sides of the fixed axis are respectively:

$$\begin{aligned} dF_p^L &= \frac{2\gamma_L \cos \theta_c}{d - r \sin \theta \sin \varphi} r dr d\varphi \\ dF_p^R &= \frac{2\gamma_L \cos \theta_c}{d + r \sin \theta \sin \varphi} r dr d\varphi \end{aligned} \quad (6)$$

where the surface energy of water γ_L varies with temperature: $\gamma_L = \gamma_{LA} = (75.6 - 0.167t)$ mJ/m² (t is celsius) (Guo et al., 2009). For micro-mechanical adhesion, surface tension is a very important force.

The torque M_p provided by the capillary force can be obtained by integrating the differential forces on the left and right with respect to the fixed axis of rotation (i.e., the torsional beam):

$$M_p = \int_0^\pi \int_0^R \left(\frac{2\gamma_L \cos \theta_c}{d - X} - \frac{2\gamma_L \cos \theta_c}{d + X} \right)^2 \cos \theta \sin \varphi dr d\varphi \quad (7)$$

where $X = r \sin \theta \sin \varphi$. In addition to capillary, vdW force and Casimir also play an important role on the surface dispersion forces when the structure size is small enough. When the main plate rotates by an angle θ , the vdW forces left dF_v^L and right dF_v^R acting on the two halves of the circular plate are, respectively:

$$\begin{aligned} dF_v^L &= \frac{\bar{A}}{6\pi(d - r \sin \theta \sin \varphi)^3} r dr d\varphi \\ dF_v^R &= \frac{\bar{A}}{6\pi(d + r \sin \theta \sin \varphi)^3} r dr d\varphi \end{aligned} \quad (8)$$

where \bar{A} is the Hamaker constant, which lies in the range of $(0.4 - 4) \times 10^{-19}$ J. The corresponding infinitesimal elements of the left dM_v^L and right dM_v^R vdW torque are:

$$\begin{aligned} dM_v^L &= \frac{\bar{A}}{6\pi(d - r \sin \theta \sin \varphi)^3} r^2 \cos \theta \sin \varphi dr d\varphi \\ dM_v^R &= \frac{\bar{A}}{6\pi(d + r \sin \theta \sin \varphi)^3} r^2 \cos \theta \sin \varphi dr d\varphi \end{aligned} \quad (9)$$

The total vdW torque M_v can be obtained by calculating the integral main plate area as:

$$M_v = \int_0^\pi \int_0^R \left[\frac{\bar{A}}{6\pi(d - X)^3} - \frac{\bar{A}}{6\pi(d + X)^3} \right] r^2 \cos \theta \sin \varphi dr d\varphi \quad (10)$$

Similarly, Casimir torque M_s can be derived as follows:

$$M_s = \int_0^\pi \int_0^R \left[\frac{\pi^2 hc_0}{240(d - X)^4} - \frac{\pi^2 hc_0}{240(d + X)^4} \right] r^2 \cos \theta \sin \varphi dr d\varphi \quad (11)$$

where $h = 1.055 \times 10^{-34}$ J·s is the reduced Plank's constant, $c_0 = 3.0 \times 10^8$ m·s⁻¹ is the speed of light.

As the main plate rotates around the torsional beam, a recovery torque M_a is generated by the beam and can be expressed as:

$$M_a = \frac{2GI_p}{l} \theta \quad (12)$$

where G , I_p and l represent the shear modulus, the polar moment of inertia and the length of the torsional beam, respectively.

The initial spacing d and tilting angle θ in the above equation are dimensionless to D and Θ :

$$D = \frac{d}{R}; \quad \Theta = \frac{\theta}{\theta_{\max}}; \quad \theta_{\max} = \arcsin \frac{d}{R} \approx \frac{d}{R} \quad (13)$$

where θ_{\max} is the maximum tilting angle.

3. Laminated piezoelectric composite structure for torsional beam

The piezoelectric effect of piezoelectric materials is divided into positive piezoelectric effect and inverse piezoelectric effect. The positive piezoelectric effect is the conversion of mechanical energy into electrical energy. When a piezoelectric material subjects to a force along a certain direction and deforms, the internal polarization phenomenon will occur, and the opposite charge will be generated on its two surfaces. Based on this positive effect, a piezoelectric material can be used as a sensing device to detect the deformation of some parts of MEMS. Conversely, the inverse piezoelectric effect is the conversion of electrical energy into mechanical energy. Specifically, the electric field applied in the polarization direction of a piezoelectric material can generate the deformation of the material. Based on this inverse effect, a piezoelectric material can be used as a driving device of MEMS. Therefore, all basic research and engineering applications on piezoelectric materials start with piezoelectric effects.

To sense the tilting angle of the main plate under the surface force and enhance the system's ability to resist pull-in instability, piezoelectric sheets were added to the torsional beam in a micromirror system, as shown in Fig. 2(a). The beam has an antisymmetric layering structure with piezoelectric sheets layers at on the upper and lower surfaces of the beam (Fig. 2(b)). The cross-sectional view of the beam with the piezoelectric sheet part laid is shown in Fig. 2(c). A torque M_{pzl} can be generated under the effect of electric field or polarization. By this antisymmetric lay-up, the parts of the piezoelectric moment formed on the upper and lower surfaces that bend the beam can cancel each other out, leaving only the torsional part.

The micromirror system is stable when the elastic restoring torque M_a , electrostatic torque M_e and surface dispersion torques (M_v , M_s or M_p) piezoelectric torque M_{pzl} are in balance. Thus, the equilibrium equation of circular torsion actuator can be expressed as:

$$2M_a + M_{pzl} = M_e + m \cdot M_v + n \cdot M_s + p \cdot M_p \quad (14)$$

where m , n and p are the torque coefficients corresponding to the surface torques. If the vdW force is considered, $m = 1$; otherwise, $m = 0$. So are the Casimir force and the capillary force. The Casimir force dominates when the initial gap between the main plate and the fixed electrodes is a few hundred nanometers, and the vdW force becomes apparent when it is a few tens of nanometers. However, capillary force is related to water in the environment and should be considered more precisely when the micromirror is in a humid environment or fabricated by wet etching methods.

Taking advantage of the piezoelectric effect, when the micromirror starts to tilt under the action of electrostatic force, the beam then twists and the piezoelectric sheets on the beam

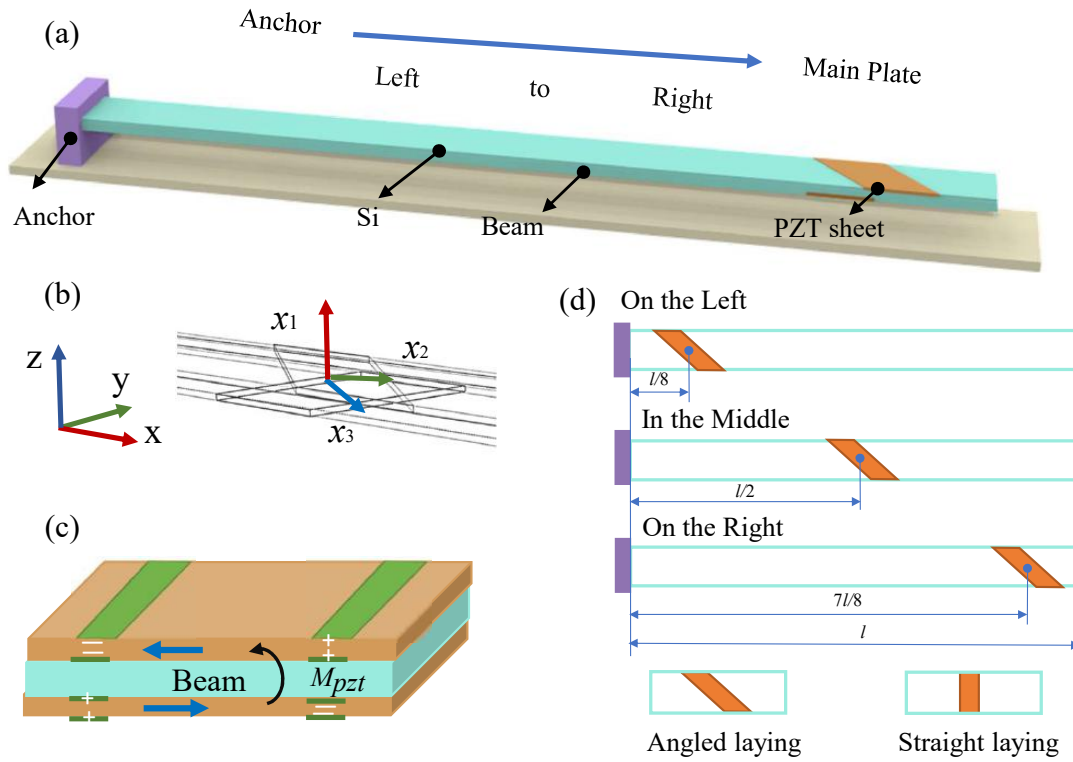


Fig. 2. Laminated torsional piezoelectric composite structure: (a) Schematic diagram of the beam with a piezoelectric sheet, (b) Global and local coordinate systems (for setting the orientation of the piezoelectric material), (c) Cross-sectional view of piezoelectric laminated structure, and (d) Top view of piezoelectric laminated structure.

deform and generate a measurable positive voltage. According to the value of the positive voltage, the tilting angle of the micromirror can be obtained finally. If the tilting angle is too large and the main plate is at the risk of pull-in instability, the inverse voltage is actively input to the piezoelectric sheets, causing a pair of piezoelectric sheets to generate a torque M_{pzt} which is opposite to the tilt direction of the main plate. The torque M_{pzt} will reduce the tilting angle of the micromirror and prevent its pull-in instability.

Additionally, the control effects of piezoelectric sheets with different positions (the center of the piezoelectric sheet (Fig. 2(d)): $l/8$, $l/2$ and $7l/8$, l is the length of the beam) and directions (the angled laying and the straight laying) on the beam were compared. Finally, the one with best effect was selected for further investigation in section 5.

4. Finite element model of electromechanical micromirror

According to the schematic model and force analysis of the micromirror in Fig. 1, a finite element simulation model is established in COMSOL, and its setting parameters are shown in Table 1. In finite element analysis, the micromirror system is mainly composed of micromirror main plate, electrode plate, torsion beam and piezoelectric plate on the beam. A micromirror main plate with a thickness of $10 \mu\text{m}$ and a radius of $200 \mu\text{m}$ was established. The thickness of the torsional beam is $10 \mu\text{m}$ and the width is $6 \mu\text{m}$. The two ends of

one beam are attached to the main plate and to the anchor, respectively, which are $100 \mu\text{m}$ from each other. The shape and size of one of the electrodes is the same as half of the micromirror, and the piezoelectric plate is in the shape of an angled parallelogram. The micromirror system is set in the global coordinate system. The piezoelectric material has different properties in different directions, so a local coordinate system is established for setting the piezoelectric material direction, as shown in Fig. 2(b). It is assumed that x_1 is perpendicular to the surface of the piezoelectric plate and x_3 is along the direction of the piezoelectric sheet also for the polarization direction of piezoelectricity.

PZT-5H is selected as the piezoelectric plate material, which is set as strain-charge type. The constraints at both ends of the beam are fixed, and the micromirror is set up as a linear elastomer. The potential difference of the piezoelectric plate is used to sense the micromirror tilting angle, and the voltage of the main plate is used to drive the micromirror. Moreover, the surface force should be considered in the system by entering the equation for the surface force per unit area on the micromirror surface using the spring basis module.

Meshing is crucial in finite element simulation process. In general, the denser the meshing, the higher the accuracy of the simulation results, and the lower the efficiency of the simulation. Thus, the effect of element quantity on the result accuracy and computational efficiency must be considered. For a simple 3D model, COMSOL Multiphysics was used to mesh it randomly by the size of elements (Table 2). To ensure both

Table 1. Setup of micromirror system in COMSOL.

| | Main plate | Beam | PZT |
|-------------------------------|---|---|--|
| Geometric parameters | $R = 200 \mu\text{m}$ $h = 10 \mu\text{m}$ | $B = 6 \mu\text{m}$ $H = 10 \mu\text{m}$ $l = 100 \mu\text{m}$ | Angled laying |
| Material parameters | $E = 160 \text{ GPa}$ $\rho = 2,330 \text{ kg/m}^3$ $\nu = 0.22$ $\varepsilon = 4.5$ | $E = 194 \text{ GPa}$ $\rho = 1,177 \text{ kg/m}^3$ $\nu = 0.2$ | PZT-5H |
| “Solid mechanics” module | Linear elastic material | Fixed at both ends of beam | Strain-charge type |
| “Electrostatic” module | Conservation of charge; The electrostatic voltage | – | Conservation of piezoelectric charge; The piezoelectric voltage |
| Multi-field coupling settings | | Machine electricity; Piezoelectric effect | |

Table 2. Mesh division information.

| Size | Number | Minimum quality | Average quality |
|--------------|---------|-----------------|-----------------|
| Standard | 31,017 | 0.02223 | 0.509 |
| Refined | 75,434 | 0.03528 | 0.546 |
| More refined | 393,295 | 0.05654 | 0.607 |

the accuracy and efficiency of computation, the “refined” division is chosen. The meshing of the micromirror system is shown in Fig. 3(a). Finally, the electromechanical force solver and piezoelectric effect solver are used to solve the problem. The solutions are obtained as follows: the distribution of the electrostatic voltage, the distribution of the capillary force on the surface of the main plate and the distribution of the tilting displacement (Figs. 3(b)-3(d)), which will be discussed in next section.

5. Results and discussion

5.1 Electromechanical stability under capillary effect

5.1.1 Comparison of torque from surface dispersion forces

The solid-liquid contact angle θ_c is an important parameter to measure the wettability of the liquid to the material surface (Fig. 4(a)). $\theta_c = 0^\circ$ is completely wetting state; $\theta_c < 90^\circ$ is the partial wetting state; $\theta_c = 90^\circ$ is the boundary of wetting or not. Eq. (7) is used to calculate the capillary torque when the contact angle is 0° to 90° at dimensionless distance $D = 0.005$ and dimensionless tilting angle $\Theta = 1 \times 10^{-3}$. As shown in Fig. 4(b), the capillary torque decreases with the increase of the contact angle. The smaller the contact angle means the greater the water droplet adhesion at the solid interface and the stronger the capillary action. In addition, as the temperature rises from 0 to 40°C , the capillary torque becomes greater, but this effect is diminished as the contact angle increases. Due to the small size of the micromirror system and the low humidity of normal air, it is assumed that the micromirror system is at the edge state of wetting or not, and the solid-liquid contact

angle is close to 90° . In this situation, the capillary torques at different temperatures are close. Here, the capillary action of the micromirror system is studied at a temperature close to room temperature of 20°C .

The vdW torque and the Casimir torque play a different role in the range of the micromirror spacing. The vdW force acts mainly in the range below a few tens of nanometers, while the Casimir force acts mainly in the range up to a few hundred nanometers. Figs. 4(c) and 4(d) compares the surface torques at different dimensionless gap and tilting angle. The results show that the Casimir torque due to quantum rise and fall is significantly larger than the vdW torque at small gap; however, when the gap is increased, the Casimir torque decreases rapidly and eventually converges to zero so does the vdW torque. In contrast, the surface torques vary with the tilting angle, and the surface torques increase significantly with the increase of the tilting angle. Both Casimir and vdW torques increase significantly at small gap or large tilting angle due to the small size of the micromirror system, which implies that the microscopic torque effect becomes more important.

The size of the micromirror system is considered on the nanometer scale, and the humidity inside the micromirror system is extremely minimal. The ratio of the capillary torque to the other two kinds of surface torques is calculated. As can be seen from Figs. 4(e) and 4(f), the capillary torque in the micromirror system is much smaller than the vdW and Casimir torques, on average 5-7 orders of magnitude smaller. Therefore, the three kinds of torques in descending order are: Casimir torque > vdW torque > capillary torque.

5.1.2 Electromechanical instability without electrostatic drive

In the absence of electrostatic drive, when the distance between the main plate and the substrate is extremely small, surface dispersion forces may lead to the instability of the micromirror. Fig. 5(a) shows the changes of tilting angle caused by the surface dispersion forces when the dimensionless gap D changes from 0 to 0.001. It can be seen that an increase in the tilting angle of the micromirror decreases with the dimensionless gap D when there is no electrostatic drive. When the gap decreases to a certain extent, the tilting angle

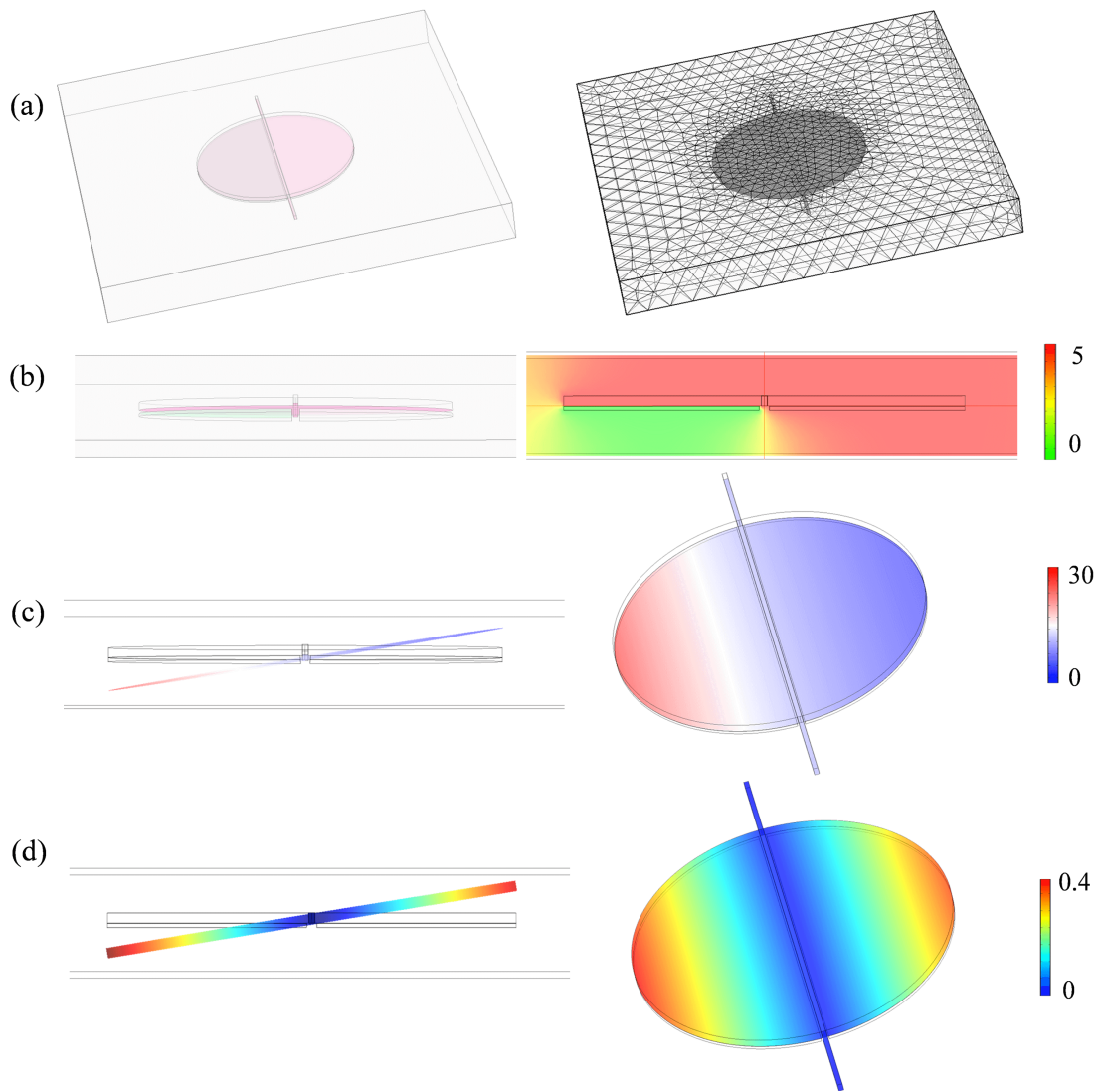


Fig. 3. Numerically modeling torsional micromirror actuator: (a) Simulation model and meshing, (b) Electric potential distribution between micromirror surfaces, (c) The capillary force distribution between micromirror surfaces, and (d) Micromirror torsional deformation displacement.

will increase rapidly. It is worth noting that the capillary effect is very small and causes a much more reduced maximum tilting angle than that caused by the vdW and Casimir forces. In any case, a sudden increase in tilting angle may lead to instability of the micromirror system. The micromirror system will suffer from pull-in phenomenon by surface forces dominating the micromirror in the absence of electrostatic driving force.

5.1.3 Electromechanical instability with electrostatic drive

Indeed, the micromirror requires an electrostatic drive in the working state. If the surface forces are considered, the micromirror is driven by both electrostatic force and surface force. The influence of the capillary on the stability of the micromirror system at the contact angle close to 90° is considered, and the results are shown in Figs. 5(b)-5(d). Fig. 5(b) shows a non-linear increase in deformation displacement with the increasing of electrostatic driving voltage at different

dimensionless gaps. The hollow point at the end of each curve represents the pull-in instability state of the micromirror system, The hollow point at the end of each curve represents the pull-in instability state of the micromirror system, which corresponds to the electrostatic voltage as the pull-in voltage $V_{pull-in}$ and the tilting angle as the critical tilting angle Θ_{cr} . Fig. 5(c) describes that the critical tilting angle increases nonlinearly with the dimensionless gap and finally tends to a constant value. It means that the influence of the surface force can be ignored when the gap of micromirror is large enough. It also shows that the capillary has a similar impact on the stability of the micromirror system to the other two surface forces when the system is driven by electrostatic voltage.

In fact, MEMS is generally influenced by Casimir and capillary force together or vdW force and capillary force together since the capillary force is influenced by environmental humidity, while Casimir force and vdW force are generated by quantum fluctuation. Therefore, the coupling effect critical

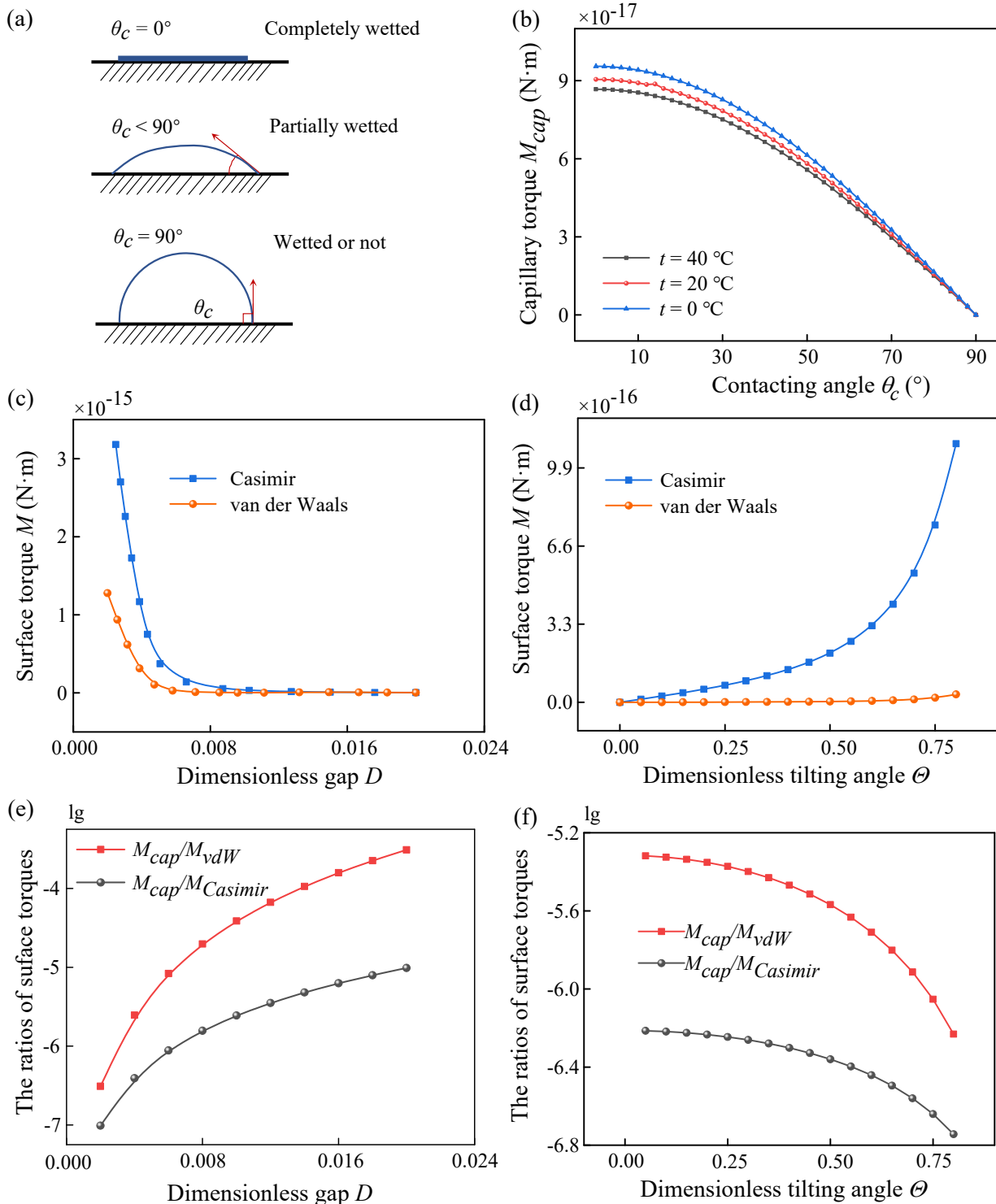


Fig. 4. Influences of capillary force on electromechanical coupling combined with vdW and Casimir forces: (a) The condition of wetting with different contact angles, (b) Change of capillary torque with solid-liquid contact angle and temperature ($D = 0.005$, $\Theta = 1 \times 10^{-3}$), (c) Change of dispersion torque with dimensionless gap ($\Theta = 1 \times 10^{-3}$), (d) Change of dispersion torque with dimensionless tilting angle ($D = 0.005$), (e) Change of the ratios of torques with dimensionless gap ($\Theta = 1 \times 10^{-3}$, $t = 20^\circ\text{C}$), and (f) Change of the ratios of torques with the dimensionless tilting angle ($D = 0.005$, $t = 20^\circ\text{C}$).

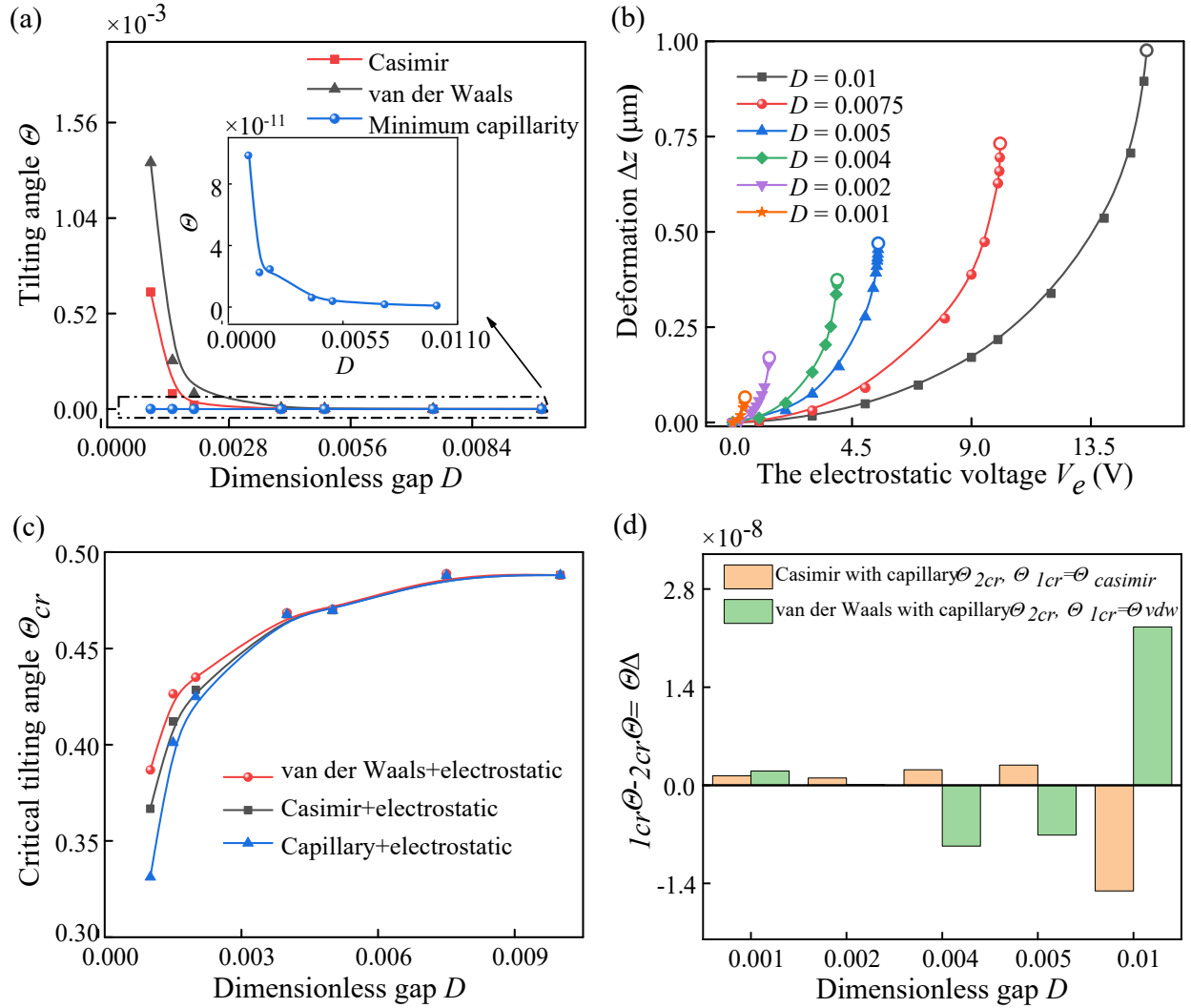


Fig. 5. Influences of capillary force on the stability of micromirror system at different electrostatic voltage V_e : (a) When $V_e = 0$, the relationship between the tilting angle and the dimensionless gap at different surface force, (b) When $V_e \neq 0$, the relationship between and micromirror deformation displacement considering capillary, (c) When $V_e = V_{pull-in}$, the relationship between the tilting angle and the dimensionless gap under capillary force with other surface forces, and (d) The difference between the tilting angle of the capillary force acting with the surface forces and the critical tilting angle of the only surface force at different gap.

tilting angle θ_{2cr} and the only effect critical tilting angle θ_{1cr} are calculated. In which the coupling effect of capillary force with Casimir force or capillary force with vdW force is considered in the calculation of θ_{2cr} . Only the effect of Casimir force or vdW force is considered in the calculation of θ_{1cr} . The difference between the two critical tilting angles, i.e., $\Delta\theta = \theta_{2cr} - \theta_{1cr}$ at different dimensionless gap is depicted in Fig. 5(d). As the increase of the gap, the capillary has a greater influence on the difference of the critical tilting angles due to the increase of the capillary force relative to the two surface dispersion forces (Fig. 4(e)). This suggests that it is necessary to consider surface forces including capillary forces in design and control of MEMS.

In conclusion, capillary force also plays an important role in the mechanical stability of MEMS like micromirror.

Therefore, the stability of micromirror system can be further optimized by considering the effect of capillary force when designing devices structure and analyzing the stability of MEMS.

5.2 Effect of piezoelectric tuning on electromechanical stability

5.2.1 Effect of PZT location

A pair of tiny piezoelectric sheets are proposed to be laid on the top and bottom surfaces of the beam, and they are anti-symmetrically distributed to form a torque without a bending moment. The piezoelectric sheets were placed on the left, middle and right part of the beam, and the piezoelectric sheets with the angled laying and the straight laying were compared. Then their positive piezoelectric voltage and the

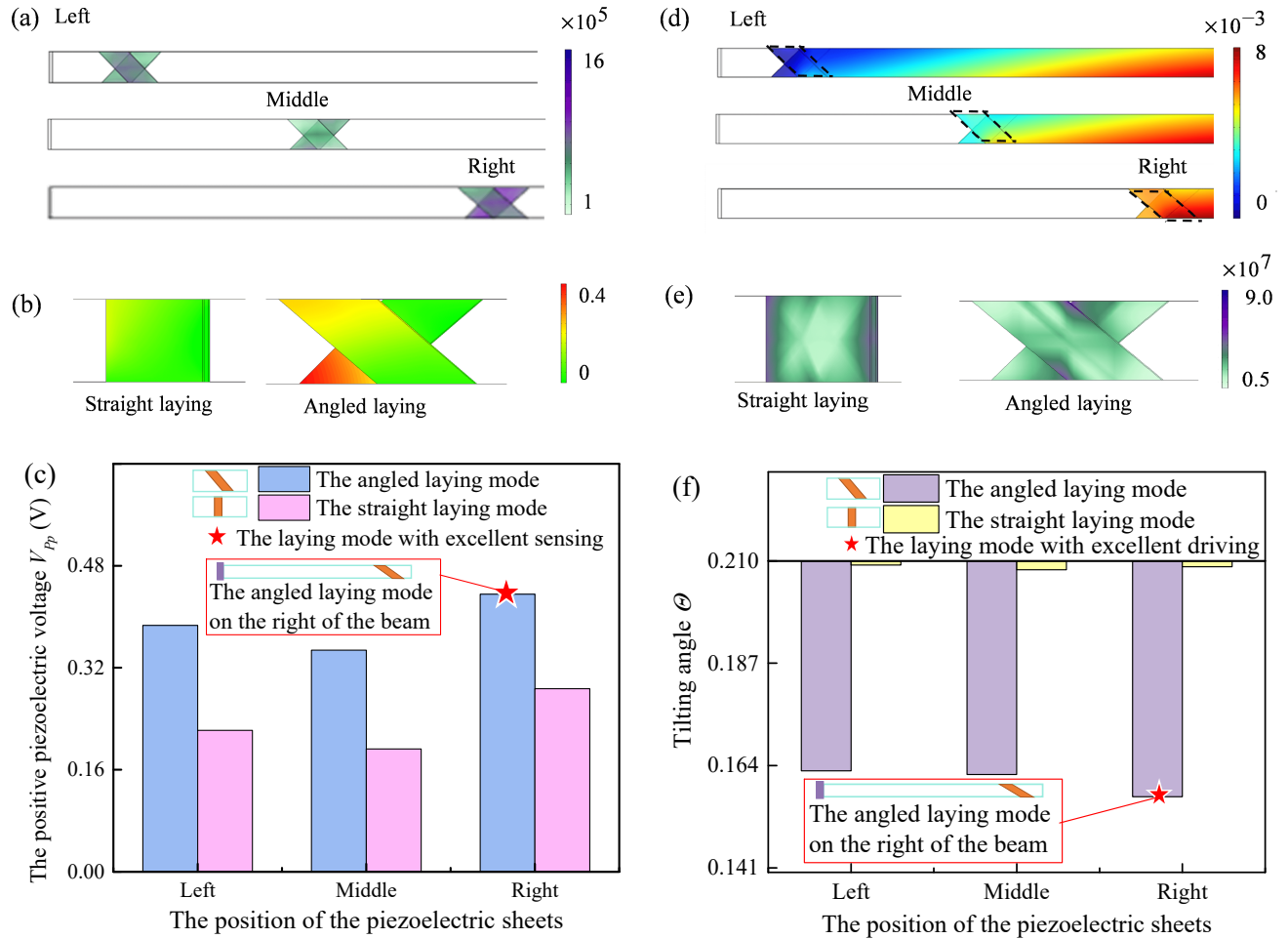


Fig. 6. The design of piezoelectric sheets. The distribution of (a) surface stress and (b) the positive piezoelectric voltage ($\Theta = 0.211$, on the right); (c) The positive piezoelectric voltage at different positions and different laying mode of the PZT sheets ($\Theta = 0.211$). The distribution of (d) the torsion displacement and (e) the surface stress ($V_{Ip} = 10$ V, $V_e = 4$ V, on the right); (f) The tilting angle for different positions and different laying mode of the piezoelectric sheets ($V_{Ip} = 10$ V, $V_e = 4$ V).

inverse piezoelectric deformation under the capillary force were analyzed. Finally, the piezoelectric laminate structure with the best piezoelectric effect was identified for subsequent studies.

The positive piezoelectric effect can sense the micromirror tilting angle. The positive piezoelectric voltage is used to predict the tilting angle of the main plate in advance so that it can prevent the micromirror from reaching the critical tilting angle and losing stability. When the micromirror is tilted at a certain angle, the positive piezoelectric voltage at different positions can be used as an indicator of the piezoelectric sensing ability. The surface stress distribution when the piezoelectric sheets are located at three different positions of the beam is shown in Fig. 6(a). When the main plate is tilted, it causes a slight bending of the beam due to the surface moment. Furthermore, one end of the beam is fixed to the anchor and the other end is fixed to the micromirror. Therefore, the surface stress should be small in the middle and large at the both ends. For the laying gesture of the piezoelectric sheet, it is allowed to lay it at an angle or at straight edge. The positive piezoelectric voltage distribution for different laying mode is shown in

Fig. 6(b). The angled laying mode has a larger voltage range, because the polarization distance of the angled laying mode is longer than that of the straight laying mode. It was calculated the positive piezoelectric voltage at different positions and different laying mode of the PZT sheets when the tilting angle $\Theta = 0.211$. From Fig. 6(c), it can be seen that the positive piezoelectric voltage V_{pp} is maximum when the piezoelectric layer is laid at the right end with an angled way, so this way of laying has an excellent sensing ability.

The inverse piezoelectric effect can drive the micromirror tilting. The micromirror will be destabilized under pull-in voltage, the inverse piezoelectric deformation can be used to weaken the tilt degree to prevent the destabilization damage. The deformation of the micromirror system caused by the inverse piezoelectric voltage differs when the piezoelectric sheets are in different positions. The tilting angle is a measure of the inverse piezoelectric driving effect. The torsional displacement of the beam with piezoelectric sheets located at three different positions can be illustrated in Fig. 6(d). Since the right end piezoelectric sheet is close to the main plate, its inverse piezoelectric deformation drives the whole main plate.

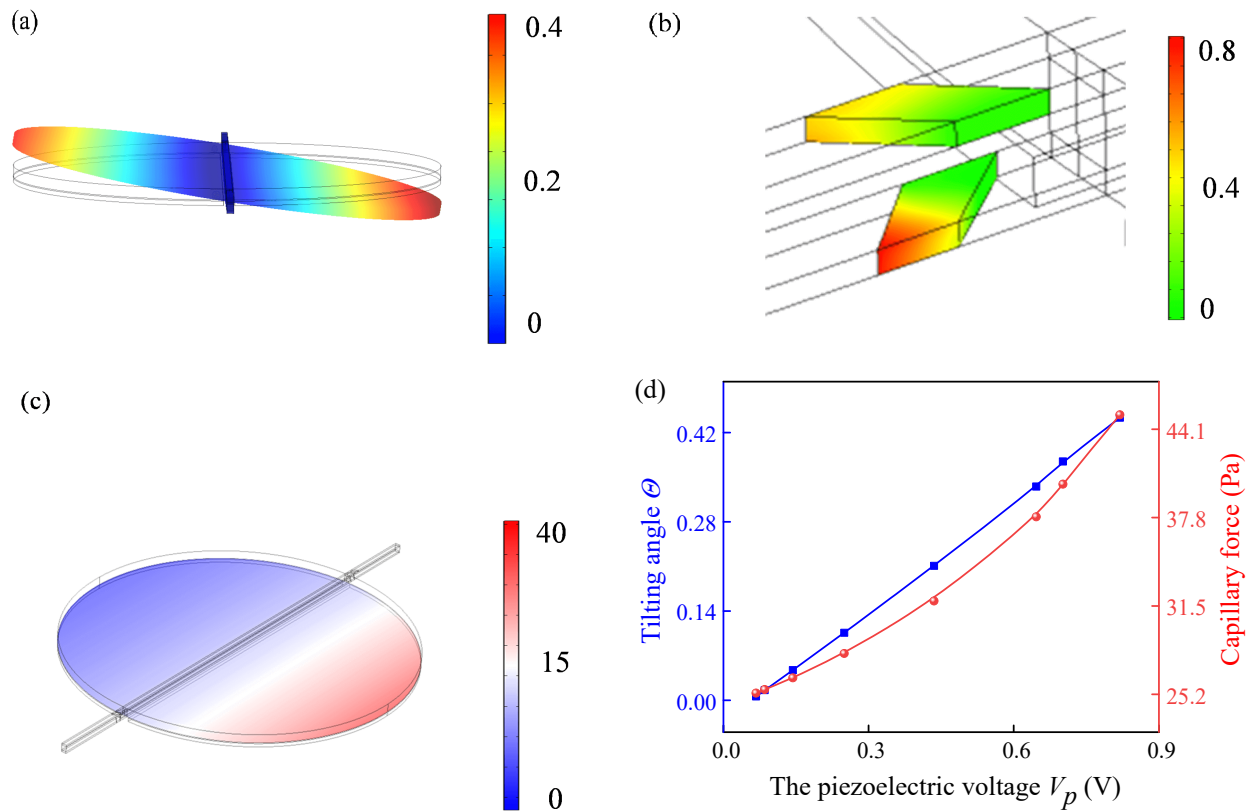


Fig. 7. The positive piezoelectric effect. The distribution of (a) the tilting displacement, (b) the positive piezoelectric voltage ($V_e = 4$ V) and (c) capillary force; (d) The variation of positive piezoelectric voltage with capillary force and tilting angle.

While the piezoelectric sheet away from the main plate, its inverse piezoelectric deformation not only drives the tilting of the main plate but also the torsion of part of the beam. Therefore, the closer the piezoelectric sheet is to the main plate, the larger the torsional displacement of the beam. The inverse piezoelectric surface stress distribution for different laying ways is shown in Fig. 6(e). The angled laying method has a greater range of surface stresses, which can cause the beam to torsion more. The tilting angle for different positions and different laying mode of the piezoelectric sheets were calculated under the inverse piezoelectric voltage $V_{Ip} = 10$ V and the electrostatic voltage $V_e = 4$ V. From the Fig. 6(f), it can be seen that the right end with an angled laying way weakens the tilt of the micromirror the most, so this laying way has a more excellent driving ability to weaken the tilting angle of the micromirror.

In summary, in order to make both the driving and sensing effects of piezoelectricity more obvious, the piezoelectric sheet was placed at the right end with an angled laying way to analyze the piezoelectric driving and sensing effects of the micromirror.

5.2.2 Sensing the tilting angle of the micromirror

When the micromirror is tilted, the torque on the beam causes polarization inside the piezoelectric sheet, along with a potential difference (the positive piezoelectric voltage V_{Pp}). Fig. 7(a) shows the tilting deformation of the main plate

under the electrostatic driving voltage $V_e = 4$ V. In this tilting deformation state, the capillary force on the main plate surface is shown in Fig. 7(c), and the positive piezoelectric voltage V_{Pp} distribution is shown in Fig. 7(b). The positive piezoelectric voltage V_{Pp} distributions of the upper and lower piezoelectric sheets are different due to the surface forces causing a slight bending of the beam, so the different torsional forces are different on the upper and lower surfaces.

It is calculated the positive piezoelectric voltage V_{Pp} under different tilting angle of the main plate. When the micromirror is in a stable state with a tilting angle, there is a unique capillary force magnitude and positive piezoelectric voltage V_{Pp} corresponding to it. According to the Fig. 7(d), a larger tilting angle and a greater capillary force both correspond to a larger positive piezoelectric voltage V_{Pp} . The former can be regarded as a linear relationship and the latter as a nonlinear relationship. By analyzing the relationship among tilting angle, capillary force and positive piezoelectric voltage V_{Pp} , the tilting degree and the external surface force of the main plate can be sensed by positive piezoelectric voltage. In this way, the instability state can be predicted in advance.

5.2.3 Resisting the pull-in instability of the micromirror

Applying an electric field (the inverse piezoelectric voltage V_{Ip}) in the polarization direction of the piezoelectric sheet can generate a stress tensor T in the corresponding direction, as shown by the white arrow on Fig. 8(a). The torque M_{pzt} is

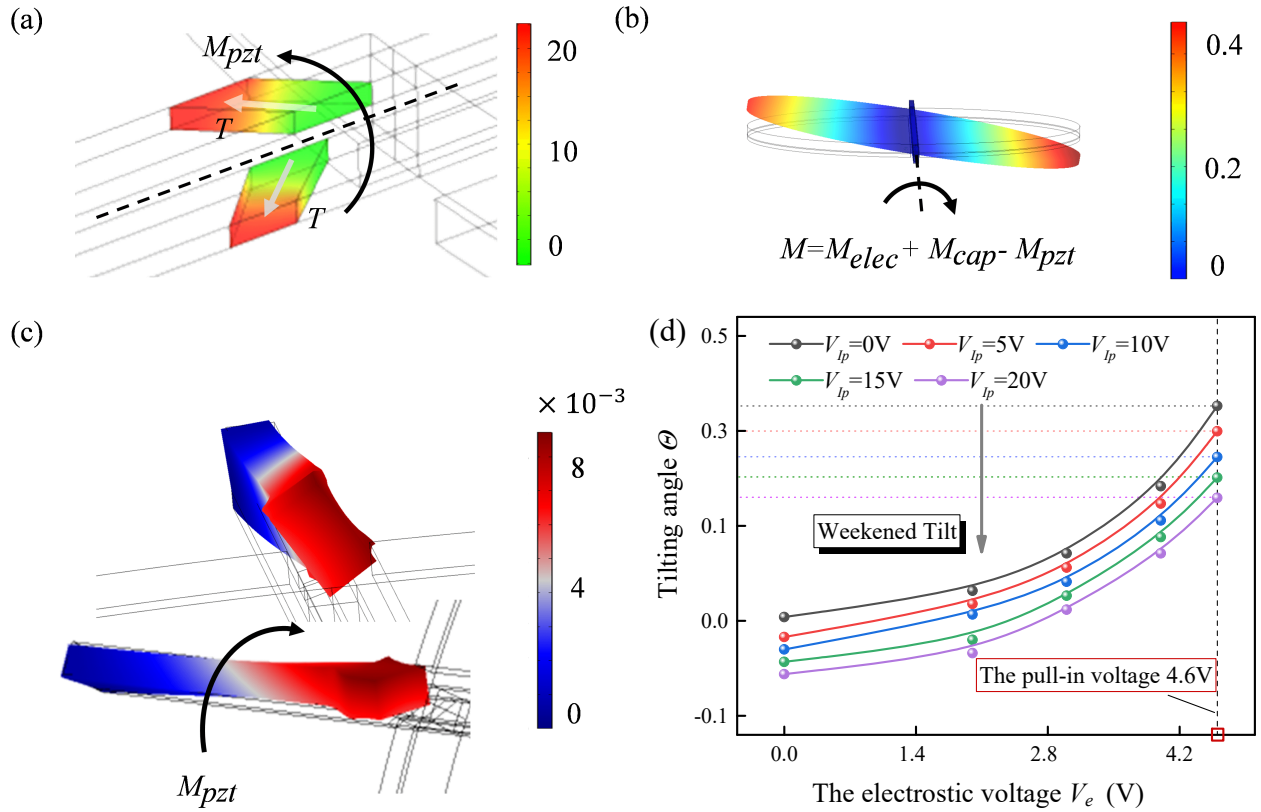


Fig. 8. The inverse piezoelectric effect: (a) The distribution of the inverse piezoelectric voltage V_{Ip} , (b) The tilting displacement of the micromirror ($V_e = 4$ V, $V_{Ip} = 20$ V), (c) The torsion displacement of the beam ($V_{Ip} = 20$ V), and (d) The relationship between the tilting angle and the electrostatic voltage V_e under different inverse piezoelectric voltage V_{Ip} .

formed by the upper and lower piezoelectric stresses relative to the neutral axis of the beam. It is in the opposite direction of the torque M_e and M_p driving the tilting of the main plate, which can weaken the tilting angle of the main plate. The torsional displacement of the beam driven by the M_{pzt} is shown in Fig. 8(c). When considering the capillary force, the tilting displacement of the main plate when the inverse piezoelectric drive and electrostatic drive act together is shown in Fig. 8(b).

From Fig. 8(d), it can be seen that the tilting angle decreases with the increase of the inverse piezoelectric voltage when the capillary force effect is considered at the same electrostatic driving voltage. Under the combined action of electrostatic and inverse piezoelectric driving together, the tilting deformation of the micromirror can be weakened. The weakening effect will be greater as the inverse piezoelectric voltage increases. When the inverse piezoelectric torque M_{pzt} is larger than the driving torque M_e and M_p , the micromirror will be reverse tilted, i.e., $\Theta < 0$. The tilting angle can also be weakened at the pull-in voltage, which can avoid pull-in destabilization and destroy the micromirror.

6. Conclusions

This paper compares the capillary force and other two surface forces on micromirror mechanical stability of the system. It is found that although the capillary force is much smaller than vdW force and Casimir force, the capillary effect

also affects the mechanical stability of micromirror system like vdW and Casimir forces, which may cause the pull-in instability of a micromirror system.

To make a micromirror system controllable and prevent it from pull-in instability, there are two piezoelectric sheets placed on the upper and lower surfaces of the torsion beam to sense the tilting angle of the main plate or drive the micromirror based on the piezoelectric effect. The relationship between the tilting angle, capillary force, and (positive/inverse) piezoelectric voltage was obtained by using finite element method. The results show that the larger the tilting angle of the micromirror is, the larger the positive piezoelectric voltage is. Therefore, the unstable state of the micromirror can be predicted in advance by reading the positive piezoelectric voltage to prevent the instability of the micromirror. On the other hand, the inverse piezoelectric effect can reduce the tilting angle, for which the critical instability of the micromirror can be reduced by adjusting the inverse piezoelectric voltage to reduce the capillary effect on the stability of the micromirror.

In summary, this article presents a comprehensive method to actively control a circular micromirror actuator to prevent its pull-in instability by applying or sensing the piezoelectric voltage in the piezoelectric composite structural beam. This work can help to optimize the design and fabrication of electromechanical micromirror system. Whereas, this design still requires specific analysis and verified in the actual application

environment. Based on the methods, a safe operating range of the micromirror can be derived, as well as a method to regulate the instability by integrating piezoelectric composite structure. Further study is needed for achieving a closed-loop control to avoid the pull-in instability of the micromirror system.

Acknowledgement

The authors acknowledge the financial support of the National Natural Science Foundation of China (Nos. 12002238 and 12102222). Research supported by The Program for Professor of Special Appointment (Eastern Scholar) at Shanghai Institutions of Higher Learning. Sponsored by Shanghai Pujiang Program (No. 2020PJD072).

Conflict of interest

The authors declare no competing interest.

Open Access This article is distributed under the terms and conditions of the Creative Commons Attribution (CC BY-NC-ND) license, which permits unrestricted use, distribution, and reproduction in any medium, provided the original work is properly cited.

References

- Afrang, S., Mobki, H., Hassanzadeh, M., et al. Design and simulation of a MEMS analog micro-mirror with improved rotation angle. *Microsystem Technologies*, 2019, 25(3): 1099-1109.
- Bhojawala, V. M., Vakharia, D. P. Closed-form relation to predict static pull-in voltage of an electrostatically actuated clamped-clamped microbeam under the effect of Casimir force. *Acta Mechanica*, 2017, 228(7): 2583-2602.
- Bhojawala, V. M., Vakharia, D. P. Investigation on pull-in voltage, frequency tuning and frequency stability of mems devices incorporating Casimir force with correction for finite conductivity. *Journal of Vibration Engineering & Technologies*, 2020, 8(6): 959-975.
- Cai, J., Chen, Y., Yang, L., et al. Capillary imbibition and flow of wetting liquid in irregular capillaries: A 100-year review. *Advances in Colloid and Interface Science*, 2022, 304: 102654.
- Cai, J., Jin, T., Kou, J., et al. Lucas-washburn equation-based modeling of capillary-driven flow in porous systems. *Langmuir*, 2021, 37(5): 1623-1636.
- Chang, J., Dommer, M., Chang, C., et al. Piezoelectric nanofibers for energy scavenging applications. *Nano Energy*, 2012, 1(3): 356-371.
- Chen, S., Yang, W., Song, J., et al. A new mechanism of energy dissipation in nanomechanical resonators due to the Casimir force. *Journal of Applied Physics*, 2019, 126(4): 044502.
- Curry, E. J., Le, T. T., Das, R., et al. Biodegradable nanofiber-based piezoelectric transducer. *Proceedings of the National Academy of Sciences*, 2020, 117(1): 214-220.
- Daichin, M., Miles, R., Towfighian, S. Lateral pull-in instability of electrostatic MEMS transducers employing repulsive force. *Nonlinear Dynamics*, 2020, 100(3): 1927-1940.
- Fang, X., Li, X., Hu, K., et al. Destructive reliability analysis of electromagnetic MEMS micromirror under vibration environment. *IEEE Journal of Selected Topics in Quantum Electronics*, 2022, 28(5): 1-8.
- Guo, J., Zhou, L., Zhao, Y. Instability analysis of torsional MEMS/NEMS actuators under capillary force. *Journal of Colloid and Interface Science*, 2009, 331(2): 458-462.
- Ico, G., Showalter, A., Bosze, W., et al. Size-dependent piezoelectric and mechanical properties of electrospun P(VDF-TrFE) nanofibers for enhanced energy harvesting. *Journal of Materials Chemistry A*, 2016, 4(6): 2293-2304.
- Jariwala, T., Ico, G., Tai, Y., et al. Mechano-responsive piezoelectric nanofiber as an on-demand drug delivery vehicle. *ACS Applied Bio Materials*, 2021, 4(4): 3706-3715.
- Khatami, F., Rezazadeh, G. Dynamic response of a torsional micromirror to electrostatic force and mechanical shock. *Microsystem Technologies*, 2009, 15(4): 535-545.
- Kumar, A., Kumar, P., Bajpai, A., et al. Design and development of a double-bridge micromirror with bending and twisting cantilevers for multiobject spectroscopy. *IEEE Transactions on Electron Devices*, 2020, 67(10): 4392-4398.
- Lamoreaux, S. K. Demonstration of the Casimir force in the 0.6 to 6 μm range. *Physical Review Letters*, 1997, 78(1): 5-8.
- Le, T. T., Curry, E. J., Vinikoor, T., et al. Piezoelectric nanofiber membrane for reusable, stable, and highly functional face mask filter with long-term biodegradability. *Advanced Functional Materials*, 2022, 32: 2113040.
- Li, Y., Yu, D., Niu, B. Prediction of spontaneous imbibition in fractal porous media based on modified porosity correlation. *Capillarity*, 2021, 4(1): 13-22.
- Liang, J., Andersen, P. Ø., Zhou, J., et al. Applications of mercury intrusion capillary pressure for pore structures: A review. *Capillarity*, 2020, 3(4): 62-74.
- Masoumi, A., Amiri, A., Vesal, R., et al. Nonlinear static pull-in instability analysis of smart nano-switch considering flexoelectric and surface effects via DQM. *Proceedings of the Institution of Mechanical Engineers, Part C: Journal of Mechanical Engineering Science*, 2021, 235(24): 7821-7835.
- Opreni, A., Boni, N., Carminati, R., et al. Analysis of the nonlinear response of piezo-micromirrors with the harmonic balance method. *Actuators MDPI*, 2021, 10(2): 21-32.
- Pal, P., Swarnalatha, V., Rao, A. V. N., et al. High speed silicon wet anisotropic etching for applications in bulk micromachining: A review. *Micro and Nano Systems Letters*, 2021, 9(1): 1-59.
- Sun, J., Li, Z., Furtado, F., et al. A microfluidic study of transient flow states in permeable media using fluorescent particle image velocimetry. *Capillarity*, 2021, 4(4): 76-86.
- Takabayashi, A. Y., Sattari, H., Edinger, P., et al. Broad-band compact single-pole double-throw silicon photonic MEMS switch. *Journal of Microelectromechanical Systems*, 2021, 30(2): 322-329.
- Tang, Y., Li, J., Xu, L., et al. Review of electrothermal micromirrors. *Micromachines*, 2022, 13(3): 429-455.
- Tian, D., Ain, Q. T., Anjum, N., et al. Fractal N/MEMS: From pull-in instability to pull-in stability. *Fractals*, 2021,

- 29(2): 2150030.
- Tian, D., He, C. A fractal micro-electromechanical system and its pull-in stability. *Journal of Low Frequency Noise, Vibration and Active Control*, 2021, 40(3): 1380-1386.
- Tian, Y., Daeichin, M., Towfighian, S. Dynamic behavior of T-beam resonator with repulsive actuation. *Nonlinear Dynamics*, 2022, 107(1): 15-31.
- van Zwol, P. J., Palasantzas, G., De Hosson, J. Th. Influence of roughness on capillary forces between hydrophilic surfaces. *Physical Review E*, 2008, 78(3): 031606.
- Wang, J., Zhang, G., You, Z. Design rules for dense and rapid Lissajous scanning. *Microsystems and Nanoengineering*, 2020, 6(1): 1-7.
- Xu, Q., Younis, M. I. Micromachined threshold inertial switches: A review. *Journal of Micromechanics and Microengineering*, 2022, 32(6): 063001.
- Yang, W., Ding, W., Liu, M., et al. A theoretical model of a flexible capacitive pressure sensor with microstructured electrodes for highly sensitive electronic skin. *Journal of Physics D: Applied Physics*, 2021, 55(9): 94001.
- Yang, W., Kang, W., Wang, X. Scale-dependent pull-in instability of functionally graded carbon nanotubes-reinforced piezoelectric tuning nano-actuator considering finite temperature and conductivity corrections of Casimir force. *Composite Structures*, 2017a, 176(9): 460-470.
- Yang, W., Li, Y., Wang, X. Scale-dependent dynamic-pull-in of functionally graded carbon nanotubes reinforced nanodevice with piezoelectric layer. *Journal of Aerospace Engineering*, 2017b, 30(3): 04016096.
- Yang, W., Li, Y., Wang, X. Tunable electromechanical coupling of a carbon nanotube-reinforced variable cross-section nanoswitch with a piezoelectric effect. *Journal of Physics D: Applied Physics*, 2016, 49(33): 335304.
- Yang, W., Liu, M., Ying, L., et al. Coupled effects of surface interaction and damping on electromechanical stability of functionally graded nanotubes reinforced torsional micromirror actuator. *The Journal of Strain Analysis for Engineering Design*, 2022, 57(5): 360-376.
- Yang, W., Yang, F., Wang, X. Dynamic instability and bifurcation of electrically actuated circular nanoplate considering surface behavior and small scale effect. *International Journal of Mechanical Sciences*, 2017c, 126: 12-23.
- Zhang, X., Koppal, S. J., Zhang, R., et al. Wide-angle structured light with a scanning MEMS mirror in liquid. *Optics Express*, 2016, 24(4): 3479-3487.